JOURNAL OF AIRCRAFT
Vol. 38, No. 5, September–October 2001

On the Structure and Attenuation of an Aircraft Wake

E. Özger,* I. Schell,* and D. Jacob†
Technical University of Aachen, 52062 Aachen, Germany

The results of an experimental investigation of the wake-vortex structure behind a swept and tapered wing with slats and flaps are presented. The wind-tunnel test is part of a project funded by the German Research Association to investigate the flow structure of wings with different flap extensions. The investigation aims at studying the characteristics of lift-generated vortices in order to find ways to attenuate dangerous wake vortex encounters for following aircraft during takeoff and landing such that an increase in airport capacity can be achieved. The wake structure is measured for different flap settings by means of hot-wire anemometry at different streamwise positions in the near field behind the wing. The measured data are evaluated to examine vortex parameters such as core radius, maximum tangential velocities, circulation distributions, turbulence levels, and maximum induced rolling moments on a following aircraft. In addition, for one flap setting means of alleviation with a wing fin at different angles of incidence mounted at the outboard flap edge region are examined. The fin causes a large increase of the vortex core and a reduction of the maximum induced rolling moment within the measured region.

Nomenclature

b	=	wing span
b_f	=	wing span of following aircraft
c	=	wing root chord
c_F	=	wing fin chord
c_L	=	lift coefficient
$c_{L\alpha}$	=	lift gradient
c_l	=	induced rolling-moment coefficient
$c_{l,\max}$	=	maximum induced rolling-moment coefficient
D	=	diameter of wind-tunnel nozzle
d_P	=	diameter of sensors
f	=	recording frequency of the hot-wire probe
h_F	=	wing fin height
L	=	length of test section
l_P	=	active length of sensors
R_c	=	core radius
Re	=	Reynolds number
t	=	measurement period
U_∞	=	freestream velocity
u, v, w	=	velocity components in x, y, z direction
u'	=	turbulence in freestream direction
V_P	=	measurement volume of the hot-wire probe
$V_{\theta,\max}$	=	maximum tangential velocity
x	=	distance in freestream direction
y	=	distance in spanwise direction
z	=	distance in vertical direction
α	=	angle of attack
Γ	=	circulation
δ_i, δ_o	=	inboard and outboard flap angle
ε_F	=	angle of incidence of wing fin
Λ	=	aspect ratio
φ	=	sweep angle
ω	=	vorticity

Introduction

THE growth of commerical aviation has placed such a demand on the air traffic system that many major airports are capacity limited and are experiencing significant traffic delays. These delays are mainly caused by the strong vortices shed by starting and landing aircraft. It is well known that the trailing wake of a lifting wing rolls up into a pair of strong, counter-rotating longitudinal vortices that persist for many spans downstream. The strength of the trailing vortices is approximately proportional to the weight of the generating aircraft, and they represent a severe atmospheric disturbance to other aircraft that happen to traverse their path. This vortex wake problem and the associated safety issues became more important because of projects like future high-capacity transport aircraft (e.g., A3XX). Important issues to be tackled are the structure of the wake in the near field and methods to influence the far-field wake to alleviate the effects of a wake vortex encounter. Therefore this paper investigates experimentally the wake structure in the near field of a swept and tapered wing for different flap settings as well as the effect of a wing fin on the wake structure and the achievable alleviation.

In the past the wake structure of unflapped wings has been investigated both experimentally[1–3] and numerically,[2,4–8] starting from simple Betz methods[4,5,8] to elaborated Navier–Stokes computations.[2,6] Experimental investigations on flapped wings are fewer in number[9–14] as a result of the higher complexity of the wake structure. In[9,10] a detailed survey of the wake structure was carried out for different flap settings but a quantitative characterization of the hazard posed on following aircraft was not performed. In contrast, Rossow[15] quantified the hazard posed to following aircraft but did not investigate the detailed structure of the wake.

The attenuation of the vortex wake is still a challenging issue although many investigations have been performed since the 1960s.[11,15–19] The prime goal is the large-scale distribution of the vorticity in the wake. Basically, this can be accomplished by influencing the lift distribution or by increasing the dispersion of vorticity.

Altering the circulation distribution on the generating wing belongs to the convectivity dominated mechanisms that were examined by several authors.[11,18] Corsiglia and Dunham[11] investigated in-flight tests the effect of unusual flap settings on the circulation distribution in the wake of a wing and its effect on the induced rolling moment on a following aircraft. The results show that the induced rolling moment behind a B747 with fully deployed inboard flap and retracted outboard flap is smaller than for the standard landing configuration.

Increasing the dispersion of vorticity by injecting additional turbulence into the wake is a viscosity-dominated mechanism.[16,17] Croom[16] investigated the effect of a spoiler and showed that the maximum induced rolling moment could be diminished significantly.

The application of the methods just mentioned would strongly constrain the aerodynamic performance of a full-scale aircraft. The

Received 31 May 2000; presented as Paper 2000-4127 at the AIAA 18th Applied Aerodynamics Conference, Denver, CO, 14–17 August 2000; revision received 5 June 2001; accepted for publication 25 June 2001.

*Research Engineer.
†Professor and Head of Institute, Institute of Aeronautics and Astronautics. Member AIAA.

investigations of Rossow[15] and Rossow et al.[19] show that the induced rolling moments on a following aircraft can be reduced to one-third by means of wing fins without great loss in lift. He attributed the alleviating effect to a convectively based dispersion of vorticity caused by the wing fins without investigating further details of the wake flow.

In the current investigation the detailed wake structure is experimentally determined for various flap settings and vortex parameters such as core radius, maximum tangential velocity, circulation, and vorticity distribution. Moreover, the rolling moment on a following wing is computed. The effect of wing fins on the wake structure is investigated in detail by comparing vortex parameters and induced rolling moments on a following wing for the configurations with and without fin. The main objective is to identify whether the attenuating effect of the wing fin is based on convective or viscous mechanisms or on both. In a previous investigation[14] the effect of different flap settings and of a wing fin on the wake flow of a rectangular wing was investigated, whereas in the current paper, the influence of different flap deflections and of a wing fin on the more complicated wake of a swept and tapered wing with slats and flaps is reported.

Experimental Setup

The measurements were performed in the Göttinger-type low-speed wind tunnel of the Institut für Luft- und Raumfahrt. The open test section has a length of $L = 3$ m and a nozzle diameter of $D = 1.5$ m. The maximum freestream velocity is $U_\infty = 75$ m/s.

In these experiments a half model mounted on a test rack was used (see Fig. 1). Suction is applied at the perforated nose of the rack to reduce boundary-layer growth on the half model symmetry plane. An electrically powered turntable is integrated within the rack to adjust the angle of attack α of the wing models. Aerodynamic forces and moments are measured by a six-components strain gauge balance. Velocities (u, v, w) in the wake of the wing are measured by means of an automatically traversed probe. The probe can be traversed in all three axis directions (x, y, z) so that velocities can be recorded in arbitrary planes perpendicular to the freestream velocity.

Figure 2 shows the wing model. It is a swept and tapered wing model with deployable slats and flaps. The wing has a span of $b = 1.35$ m and a root chord of $c = 0.276$ m. The sweep angle of the leading edge is $\varphi = 34$ deg, and the aspect ratio amounts to $\Lambda = 8.8$. The wing profile is a BAC 3-11/RES/30/21 profile with a typical shape for transonic speeds. The flap section consists of two segments, an inboard and an outboard flap, that can be deployed independently at $\delta_i, \delta_o = 0, 10, 20$ deg.

For the configuration with retracted flaps, the slats were also retracted, whereas for all configurations with deployed flaps they were fully deployed at 25 deg. The open jet boundary can be considered to be sufficiently small and does not influence the wake flow of the investigated configurations.

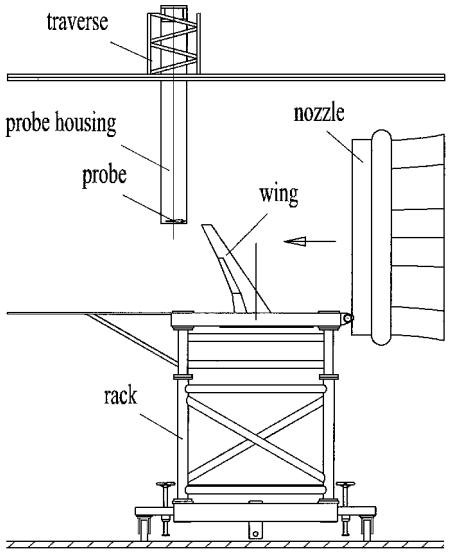

Fig. 1 Experimental rack in open test section.

Table 1 Measured cases

Angle of attack α, deg		
Force measurements	Wake measurements	Flap angle, deg δ_i/δ_o
−10–10	4/8	0/0
−10–10	4/8	10/10
−10–10	4/8	20/20
−10–10	4/8	20/10

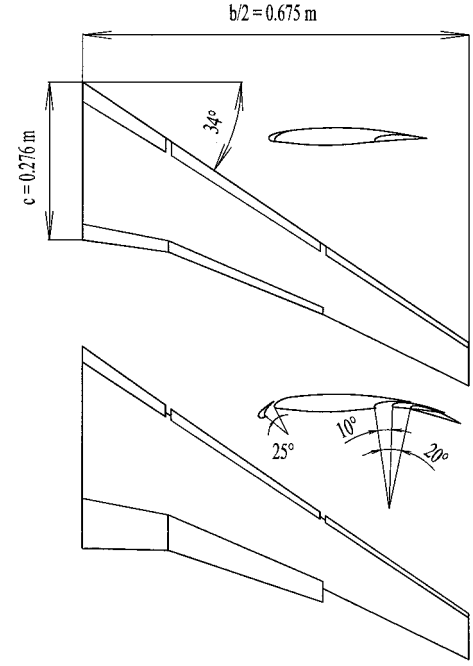

Fig. 2 Sketch of the wing model.

At first, force measurements and oil painting visualizations were conducted for each configuration to ensure that no major separation occurs and to analyze the flow structure on the suction side of the wing. Moreover smoke was injected at the wing tip and the flap edge to get a three-dimensional view of the vortices in the wake.

Then velocity measurements were performed by means of hot-wire anemometry. The three-dimensional hot-wire probes have a diameter of the sensors of $d_P = 5\ \mu$m and an active length of $l_P = 1$ mm so that the measurement volume of the hot-wire probe is about $V_P = 1$ mm^3. The velocity data were recorded at a frequency of $f = 1$ kHz for a measurement period of $t = 1$ s.

The velocities downstream of the wing were measured in planes perpendicular to the freestream velocity at four distances x based on the span b of the complete wing: $x/b = 0.0$, 0.2, 0.4, and 0.8. First, planes with a coarse step size ($\Delta y = \Delta z = 7.5$ mm) were measured to evaluate the positions of the vortices and to get an overall impression of the wake structure. Then, grids with a fine step size ($\Delta y = \Delta z = 2$ mm) were used to resolve finer structures of the vortices. In Fig. 3 the coordinate system and the investigated areas are shown. The wing is displayed with a wing fin (height h_F, chord c_F, and angle of incidence ε_F) at the flap edge position.

Wake-Vortex Structure at Different Flap Settings

Testing Program

Table 1 shows the investigated cases that will be discussed in the following. The experiments were performed at a freestream velocity of $U_\infty = 40$ m/s without fixed transition and a Reynolds number based on the root chord c of about $Re_c = 8 \times 10^5$. Force measurements were conducted at an angle of attack range between $\alpha = -10$ to 10 deg. For the wake-vortex investigation two moderate angles of

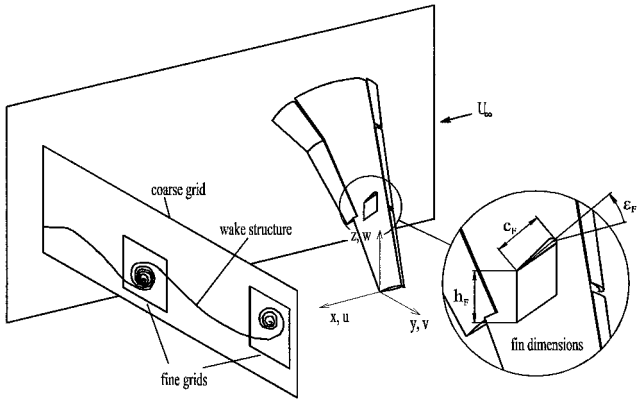

Fig. 3 Wing and wing fin with coordinate system and arrangement of measured planes.

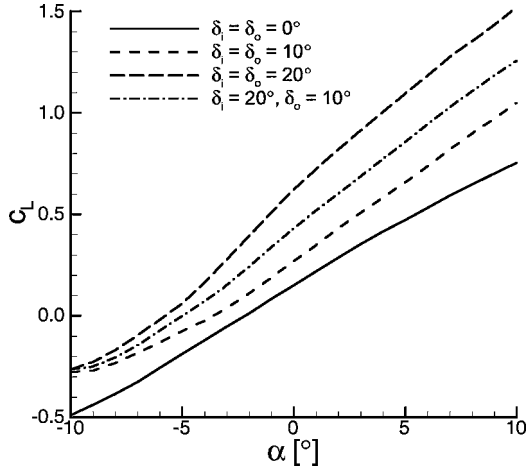

Fig. 4 Lift curves c_L for various flap settings.

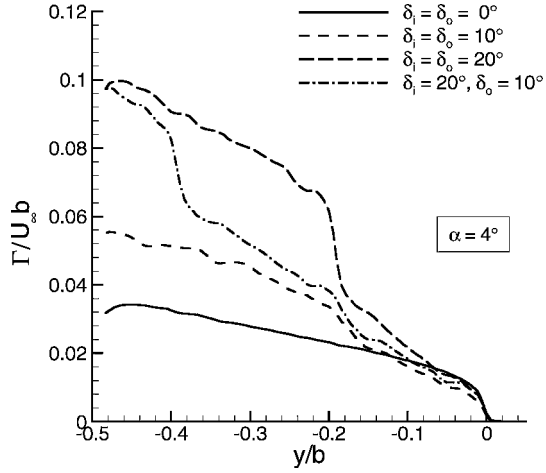

Fig. 5 Circulation distribution $\Gamma/U_\infty\, b$ for various flap settings at $\alpha = 4$ deg.

attack ($\alpha = 4$ and 8 deg) were chosen to ensure that no severe flow separation occurs for all flap configurations.

Results

The lift curves are shown in Fig. 4. For positive angles of attack, the curves show approximately linear behaviour. Deploying the flap increases both the lift and its gradient. The velocity data were evaluated to compute the circulation Γ in the wake of the wing according to

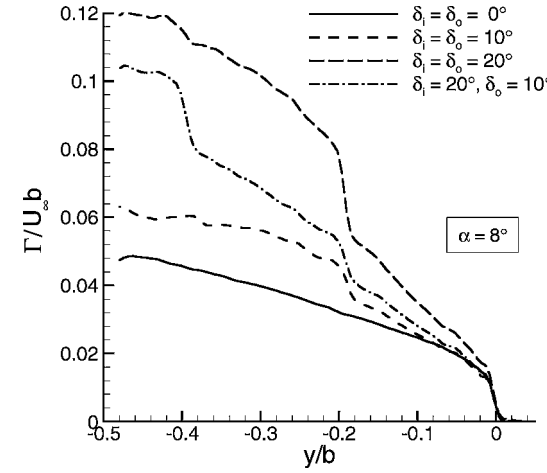

Fig. 6 Circulation distribution $\Gamma/U_\infty\, b$ for various flap settings at $\alpha = 8$ deg.

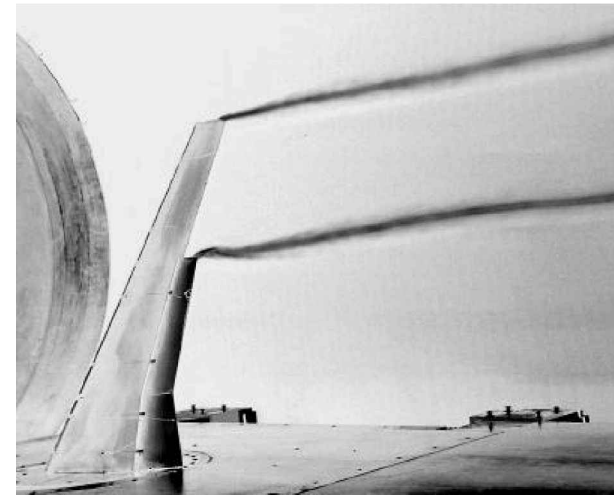

Fig. 7 Smoke visualization of the wing tip and flap edge vortex for $\delta_i = \delta_o = 20$ deg at $\alpha = 8$ deg.

$$\Gamma = \oint \boldsymbol{v} \cdot \boldsymbol{ds} \tag{1}$$

along the outer contour of the coarse grid. Figures 5 and 6 show the circulation distributions at the trailing edge of the various configurations for $\alpha = 4$ and 8 deg. The circulation distributions are consistent with the measured lift data according to the Kutta–Joukowsky theorem.

The flow visualization by means of oil painting and smoke injection showed that apart from small regions of separation behind the slat and flap supports caused by their wakes the flow on the wing is attached for any configuration in this investigation and that the wing tip and flap edge vortex are concentrated and do not decay within the test section (see Fig. 7).

The vorticity ω can be computed from the velocity data according to

$$\omega = \frac{\partial w}{\partial y} - \frac{\partial v}{\partial z} \tag{2}$$

Typical nondimensional vorticity distributions $\omega c/U_\infty$ in several planes measured in the wake of the wing with a flap setting of $\delta_i = \delta_o = 20$ deg at $\alpha = 8$ deg are shown in Fig. 8. The wake of the wing is rolling up into two stable vortices, the wing tip vortex and the outboard flap vortex. For a more detailed evaluation of the vortex parameters, the region of the vortices were measured with a smaller step size of $\Delta y = \Delta z = 2$ mm. In Figs. 9 and 10 the vorticity distribution of both vortices is shown in the planes $x/b = 0.0$, 0.2,

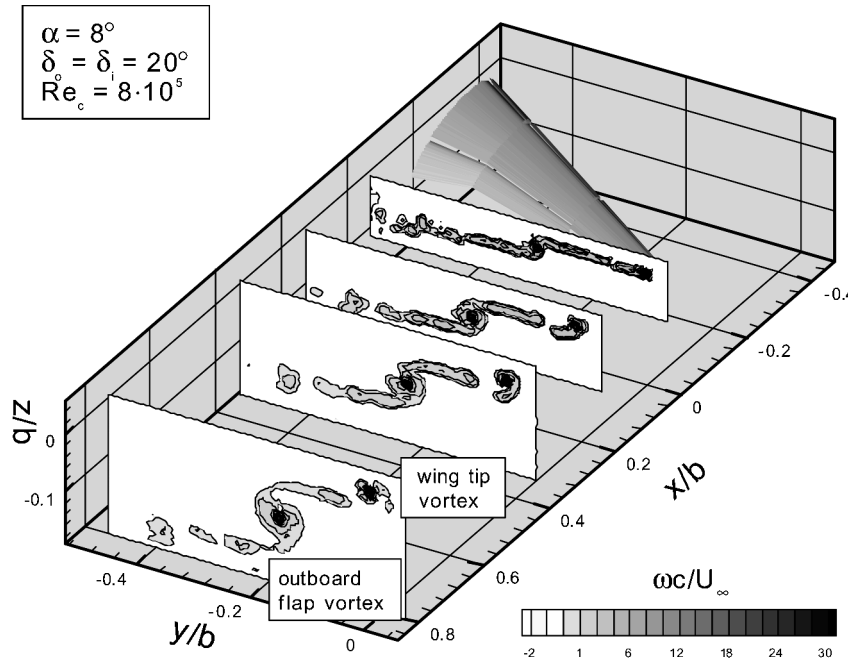

Fig. 8 Vorticity distribution $\omega c/U_\infty$ in the wake of the wing for $\delta_i = \delta_o = 20$ deg at $\alpha = 8$ deg.

0.4, and 0.8. The wing tip vortex shows a single branched structure with two vorticity maxima in the vortex center at $x/b = 0.0$ (only one vorticity maximum at $\alpha = 4$ deg), which merge into one maximum downstream. The outboard flap vortex shows a double branched structure with only one vorticity maximum defining the vortex center. The maximum vorticity is decreasing downstream for both vortices while the change in size is negligible. Moreover, the flap vortex is larger in size and shows higher values of vorticity compared to the wing tip vortex.

Important vortex parameters such as core radius R_c and maximum tangential velocity $V_{\theta,\max}$ are evaluated from the velocity data measured with the fine grids. The vortex center is defined as the locus of the maximum vorticity; the core radius is defined by the location of the maximum induced tangential velocities. Figures 11 and 12 show the core radius R_c and the maximum tangential velocity $V_{\theta,\max}$ for the wing tip and the outboard flap vortex at different downstream positions. At $\alpha = 4$ deg the core radius of the wing tip vortex is highly dependent on the deflection of the slats and flaps (Fig. 11). Deploying the slats influences the wing tip vortex caused by the interference of the high amount of turbulence in the wake of the slats with the wing tip flow. This leads to an increase of the core radius and a corresponding decrease of the maximum tangential velocities of the tip vortex. Increasing the flap angles δ_i and δ_o raises the amount of the circulation within the wing tip vortex making the vortices more resistant towards the diffusing influence of turbulence. Therefore the core radius diminishes while the maximum tangential velocity increases, both approaching the value for the configuration with retracted slats and flaps. At $\alpha = 8$ deg the core radius is constant for all flap settings and slightly higher compared to the configuration with retracted slats and flaps at $\alpha = 4$ deg. The constancy of the core radius can be explained by the fact that the flow around the slats is less detached and so the level of turbulence in the wake is lower. In addition, the amount of circulation is increased as a result of the higher lift. Because of the higher circulation and the constant core radius, the maximum tangential velocities increase correspondingly. As expected, an outboard flap angle of $\delta_o = 10$ deg produces a weaker flap vortex than an outboard flap angle of $\delta_o = 20$ deg as the lower tangential velocities for $\delta_o = 10$ deg show (Fig. 12). The weaker vortex diffuses more rapidly downstream showing a larger core radius. For an angle of attack of $\alpha = 8$ deg, the diffusion downstream is less pronounced compared to $\alpha = 4$ deg because of the higher level of circulation within the flap vortex.

To measure the hazard of the vortex wake posed to following aircraft, the induced rolling moment is computed for the experimental data according to

$$c_l = \frac{2}{b_f^2} \int_{-b_f/2}^{b_f/2} c_{L\alpha} \cdot \arctan\left(\frac{w}{u}\right) \cdot \xi \cdot \mathrm{d}\xi \tag{3}$$

The induced rolling-moment coefficient c_l is computed by means of the strip theory, where the following wing is divided into a series of chordwise strips. Each strip is treated as a two-dimensional airfoil, and the lift induced by the wake of the generator aircraft is computed as a function of the local flow angle, which is obtained from the measured velocitiy components u and w. Together with the lift gradient $c_{L\alpha}$ and a lever arm ξ, the incremental rolling moment is integrated on the whole following span b_f. Here, a span ratio of $b_f/b = 0.2$ is chosen, which is a typical ratio for such an investigation.[15,17,19]

Figure 13 shows a typical induced rolling-moment distribution in the wake of the wing at a distance of $x/b = 0.8$ for different positions of the following aircraft.

As expected, the maximum rolling moments are encountered in the region of the wing tip and outboard flap vortex. Especially, in the near-field region of the wake two components inducing the rolling moment on a following aircraft have to be distinguished. One part is generated by the downwash of the bound vortices of the wing, which fades away at large distances to the wing. The other part is generated by the downwash of the trailing vortices that are rather persistent in the wake flow up to many spans behind the wing.

From the induced rolling-moment distribution of the measured field, the maximum is evaluated. In Fig. 14 the maximum induced rolling moment $c_{l,\max}$ on the following aircraft related to the wing lift c_L of the generating aircraft is presented as a function of the distance to the trailing edge of the wing. The maximum induced rolling moment of all configurations does not change significantly downstream in the investigated wake field. For both angles of attack, the configuration with retracted slats and flaps shows the highest values of maximum induced rolling moment related to the wing lift. This can be explained by the fact that for this configuration the circulation in the wake is rolled up into one wing tip vortex, whereas for the other configurations with deployed flaps the circulation in the wake is divided into two vortices (three vortices for $\delta_i = 20$ deg, $\delta_o = 10$ deg). This division leads to a reduction of the maximum

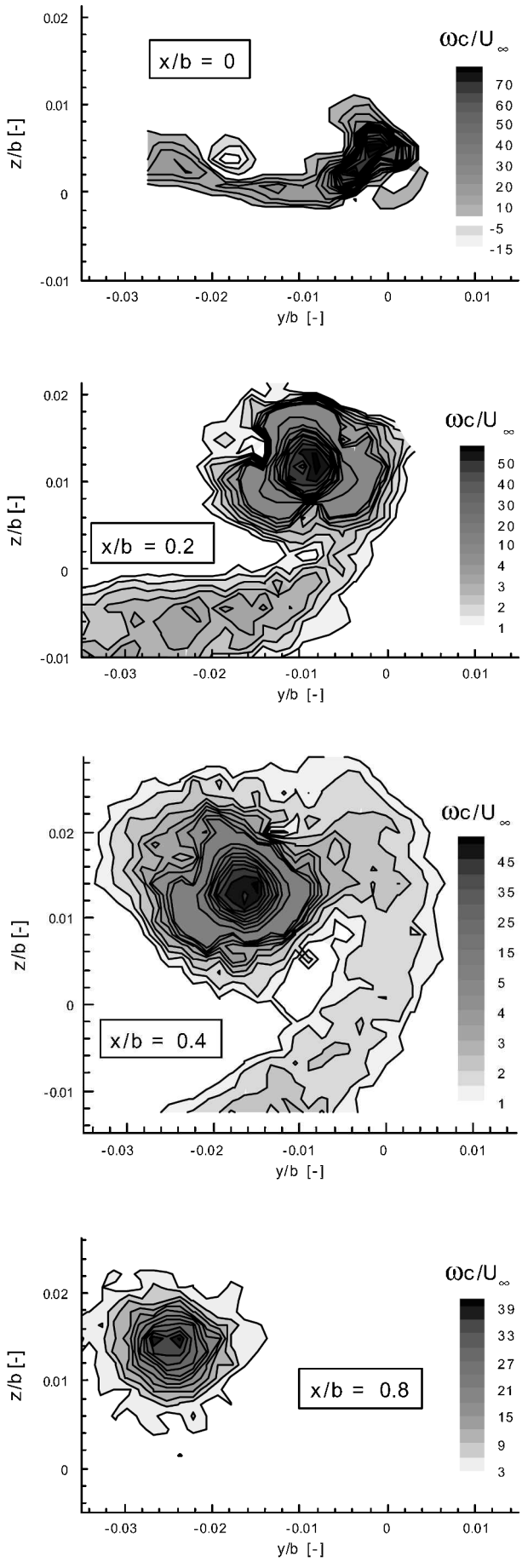

Fig. 9 Vorticity distribution $\omega c/U_\infty$ of wing tip vortex at $x/b = 0.0, 0.2, 0.4$, and 0.8 for $\delta_i = \delta_o = 20$ deg at $\alpha = 8$ deg.

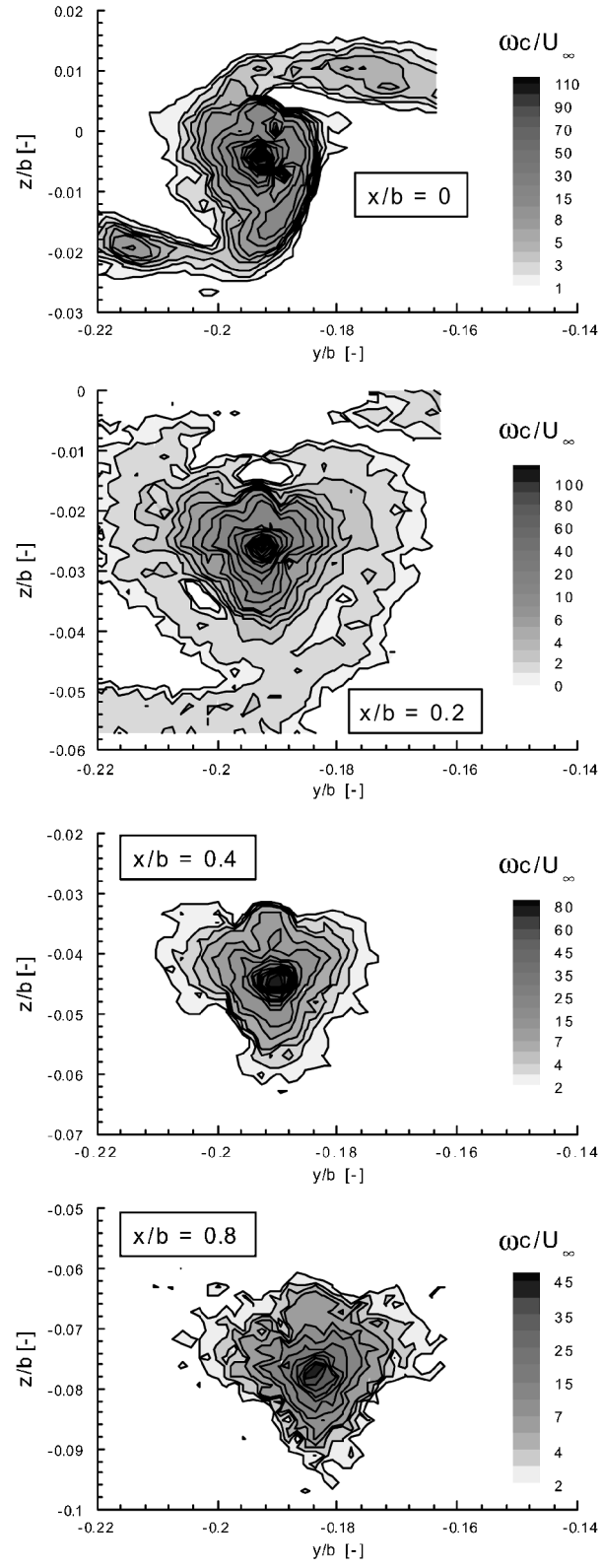

Fig. 10 Vorticity distribution $\omega c/U_\infty$ of outboard flap vortex at $x/b = 0.0, 0.2, 0.4$, and 0.8 for $\delta_i = \delta_o = 20$ deg at $\alpha = 8$ deg.

induced rolling moment related to the lift, at least in the investigated wake field up to $x/b = 0.8$, where no vortex merger of the flap and tip vortex occured.

If the circulation in the wake is distributed more equally on the vortices, the maximum induced rolling moment related to the lift shows the smallest values. This is true for the configurations with moderate flap deflection ($\delta_i = \delta_o = 10$ deg, two vortices, and $\delta_i = 20$ deg, $\delta_o = 10$ deg three vortices). Higher flap deflections, e.g.,

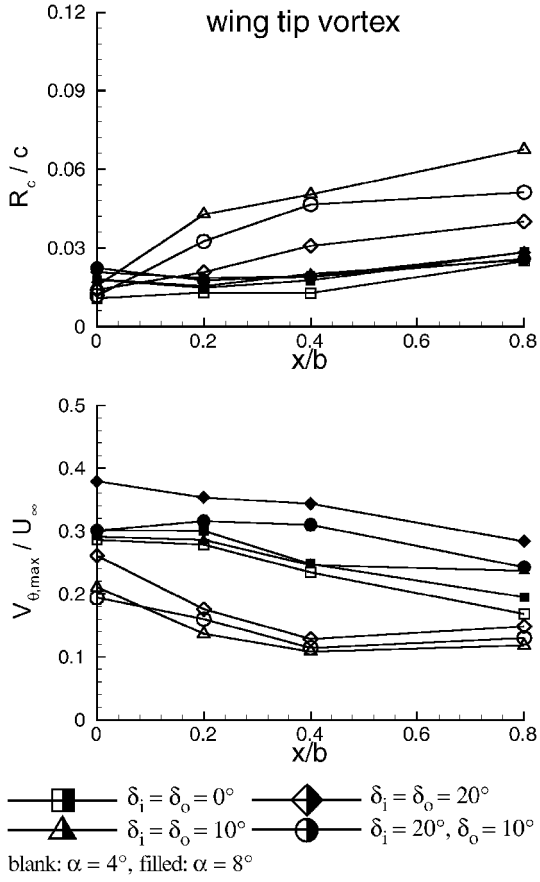

Fig. 11 Core radius R_c/c and maximum tangential velocity $V_{\theta,\max}$ for the wing tip vortex.

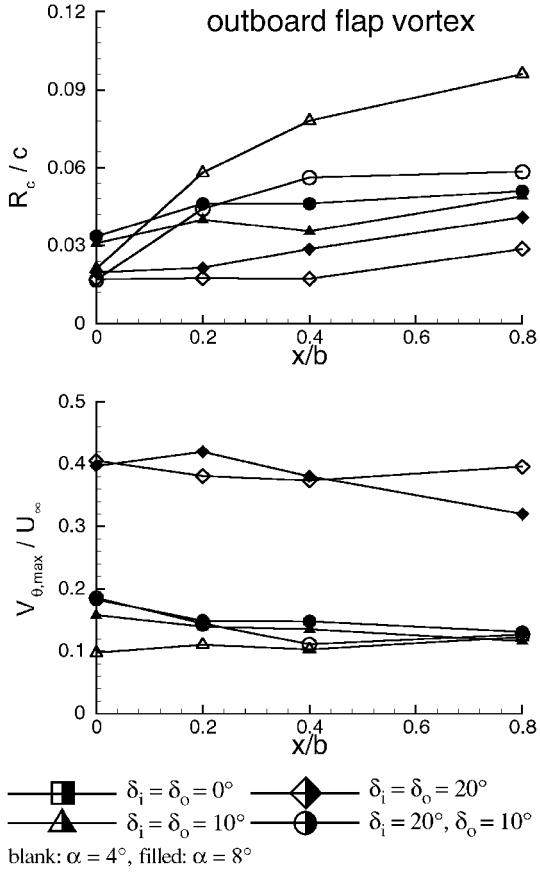

Fig. 12 Core radius R_c/c and maximum tangential velocity $V_{\theta,\max}$ for the outboard flap vortex.

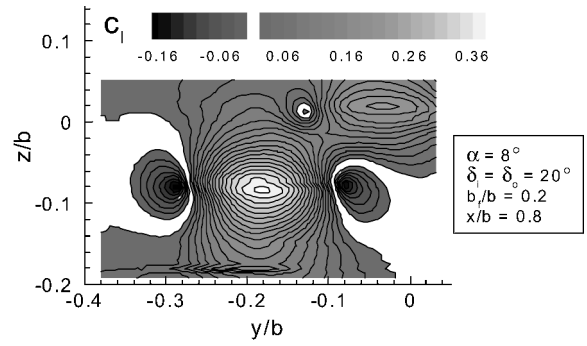

Fig. 13 Distribution of the rolling moment c_l induced on a following aircraft at $x/b = 0.8$ for $\delta_i = \delta_o = 20$ deg at $\alpha = 8$ deg.

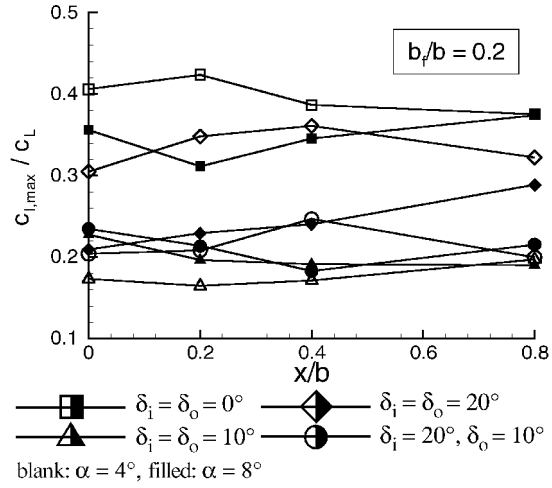

Fig. 14 Maximum induced rolling moment $c_{l,\max}$ related to the wing lift c_L on the following aircraft (wings horizontal) vs distance to the trailing edge.

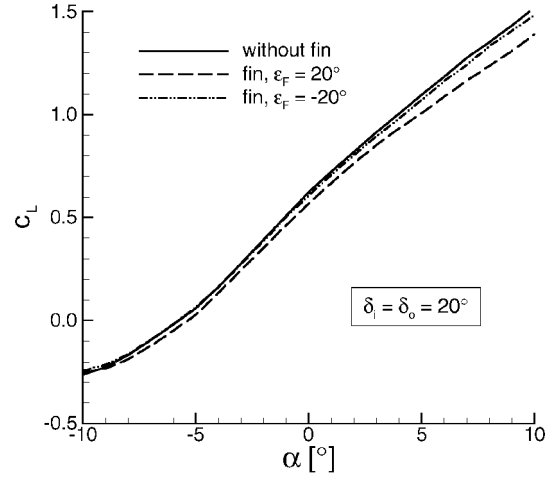

Fig. 15 Influence of fin on lift.

flap angles of $\delta_i = \delta_o = 20$ deg, produce a flap vortex that is much stronger than the tip vortex so that the maximum induced rolling moment is dominated by the flap vortex.

Alleviation of Wake Vortex by Means of Wing Fins

Testing Program

In this chapter alleviation by means of a wing fin is explored where the configuration with flap angles $\delta_i = \delta_o = 20$ deg is taken as reference. In Fig. 3 a sketch of the wing with the wing fin is shown (height h_F, chord c_F, angle of incidence ε_F). The wing fin

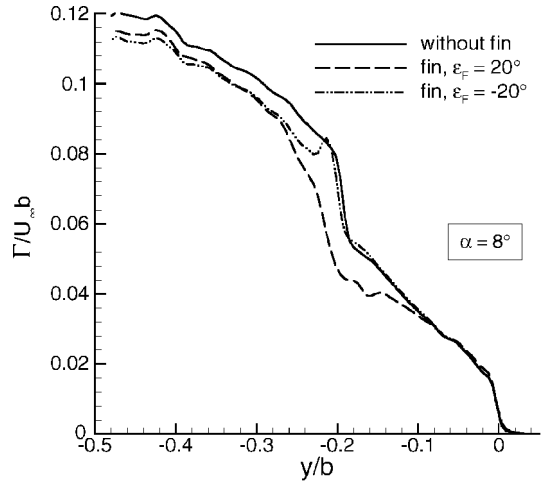

Fig. 16 Distribution of circulation $\Gamma/U_\infty\, b$ of the configurations with fin compared with the reference configuration without fin at $\alpha = 8$ deg.

Fig. 17 Smoke visualization of the wing tip and flap edge vortex for $\delta_i = \delta_o = 20$ deg at $\alpha = 9.53$ deg with fin at $\varepsilon_F = 20$ deg.

($c_F/b = h_F/b = 0.04$) was mounted at a spanwise position corresponding to the outer flap edge at two different angles of incidence ($\varepsilon_F = -20$ and 20 deg). The testing program is summarized in Table 2.

Results

The influence of the wing fin on the overall lift coefficient is shown in Fig. 15. The curves show that the largest lift decrease of 7% occurs for the fin with the positive angle of incidence (The evaluation of the experiments were conducted for constant lift, i.e., the loss in lift was compensated by increasing the angle of attack.). The influence of the fin on the circulation distribution as shown in Fig. 16 is correspondingly small.

The influence of the wing fin with positive angle of incidence on the wake flow can be seen by means of smoke visualization. Figure 17 displays the wing tip and flap edge vortex of the wing without fin. Both the wing tip and flap edge vortex are concentrated and do not decay within the test section. Because of the camera position, the wing tip and flap vortex seem to move outwards in spanwise direction which is an optical deception. Figure 17 displays the wing tip and flap edge vortex of the wing with fin ($\varepsilon_F = 20$ deg). Because of the wake of the wing fin, the flap vortex diffuses rapidly downstream while the wing tip vortex is hardly influenced by the fin.

The wake of the wing fin consists of a fin tip vortex whose sense of rotation depends on the angle of incidence ε_F (same rotation as the wing tip vortex for positive ε_F) and of a necklace vortex at the base of the fin. In Fig. 18 the vorticity distribution $\omega c/U_\infty$ in planes perpendicular to the freestream velocity behind the wing with fin is shown and is computed from the measured velocities v and w in the wake. The necklace or horseshoe vortex that wraps around the root of the wing fin could not be resolved sufficiently in the measurements. The additional vorticity in the outboard flap vortex

Table 2 Measured cases

Angle of attack α, deg		Flap angle, deg		Fin angle of incidence, deg
Force measurements	Wake measurements	δ_i/δ_o	Fin size c_F/b, h_F/b	ε_F
−10–10	9.53	20/20	0.04	20
−10–10	8.27	20/20	0.04	−20

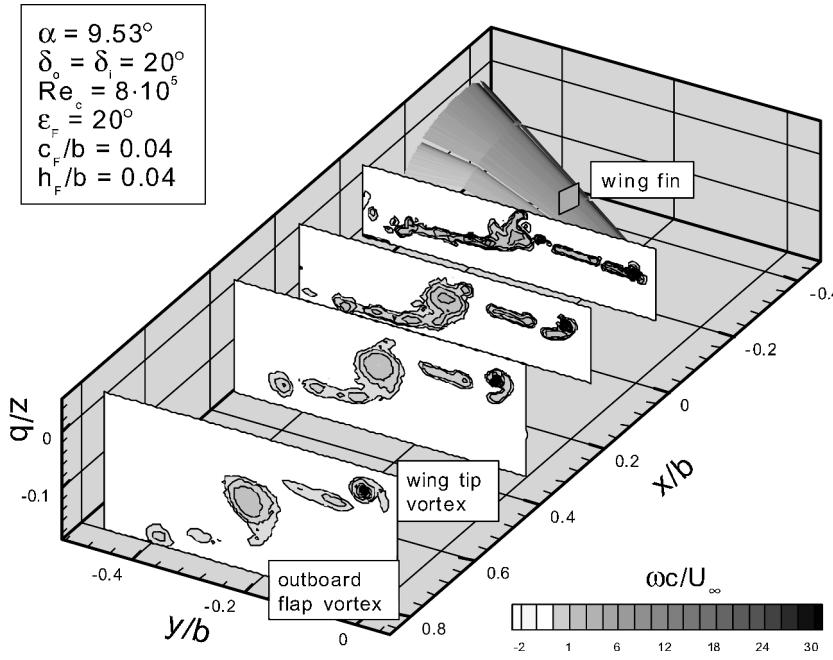

Fig. 18 Vorticity distribution $\omega c/U_\infty$ in the wake of the wing for $\delta_i = \delta_o = 20$ deg at $\alpha = 9.53$ deg with fin at $\varepsilon_F = 20$ deg.

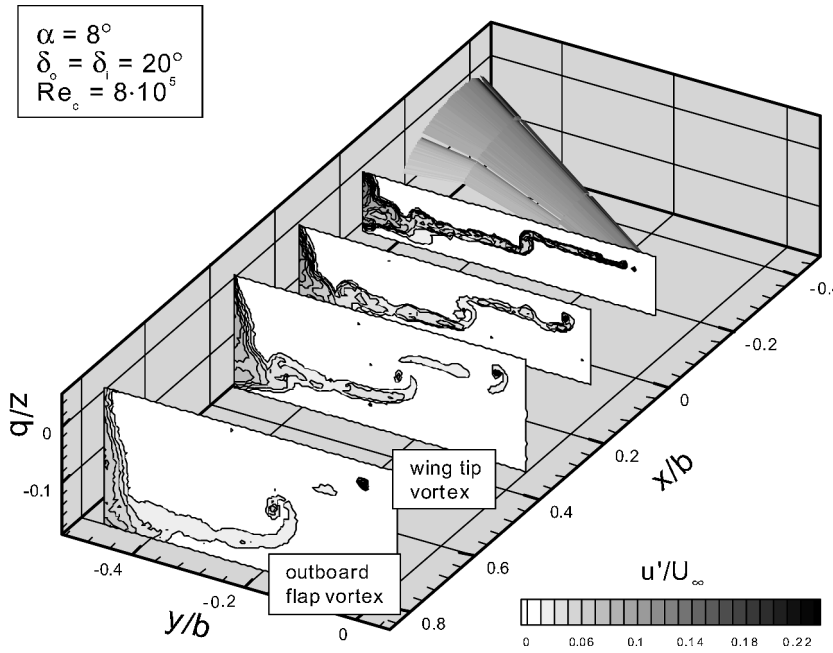

Fig. 19 Turbulence distribution u'/U_∞ in the wake of the wing for $\delta_i = \delta_o = 20$ deg at $\alpha = 8$ deg.

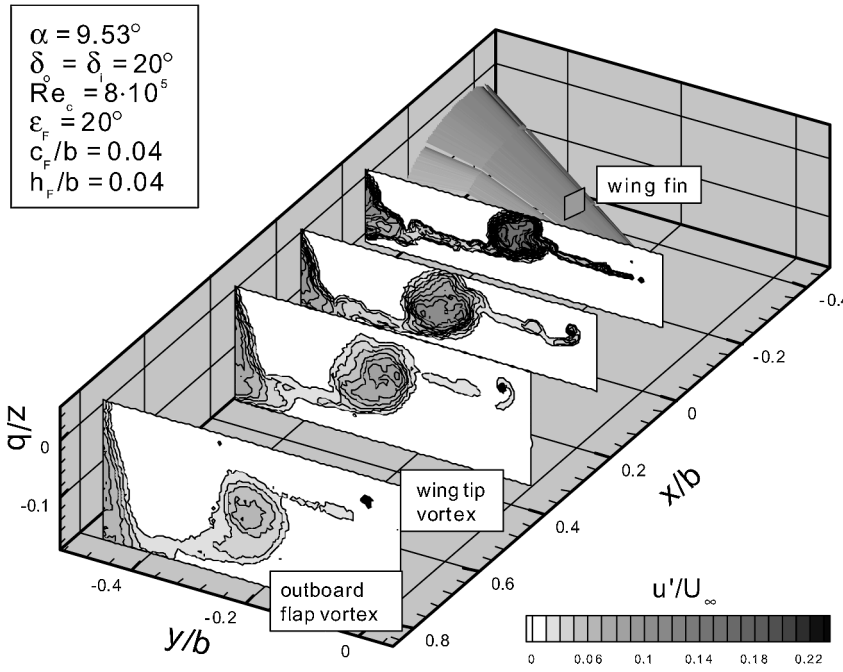

Fig. 20 Turbulence distribution u'/U_∞ in the wake of the wing for $\delta_i = \delta_o = 20$ deg at $\alpha = 9.53$ deg with fin at $\varepsilon_F = 20$ deg.

region produced by the wing fin can be seen at the first station $x/b = 0.0$ by comparing Figs. 18 and 8. The wing fin leads also to diffusion of the vorticity downstream of the region, where it is mounted as already stated by the smoke visualization in Fig. 17. The increased diffusion of vorticity in the outboard flap region is caused mainly by the higher level of turbulence generated by the partially separated flow behind the wing fin. The difference in the turbulence level between the cases without and with wing fin can be seen in Figs. 19 and 20, which show the turbulence distribution u'/U_∞ in freestream direction.

The amount of wake diffusion can be quantified by determining the influence of the wing fin on the core radius R_c and on the maximum tangential velocity $V_{\theta,\max}$. In Fig. 21 these values are presented according to

$$\Delta R_c = \frac{R_{c,\text{with fin}} - R_{c,\text{without fin}}}{R_{c,\text{without fin}}} \tag{4}$$

$$\Delta V_{\theta,\max} = \frac{V_{\theta,\max,\text{with fin}} - V_{\theta,\max,\text{without fin}}}{V_{\theta,\max,\text{without fin}}} \tag{5}$$

For $\varepsilon_F = 20$ deg the fin causes an increase of the core radius of the flap vortex by more than 200%, whereas for $\varepsilon_F = -20$ deg almost no change of the core radius occurs. The widening of the flap vortex leads to a corresponding decrease in maximum tangential velocity as shown in Fig. 21. Therefore the configuration with fin at an angle of incidence of $\varepsilon_F = -20$ deg causes almost no decrease in maximum tangential velocity at $x/b = 0.8$, whereas a decrease of maximum

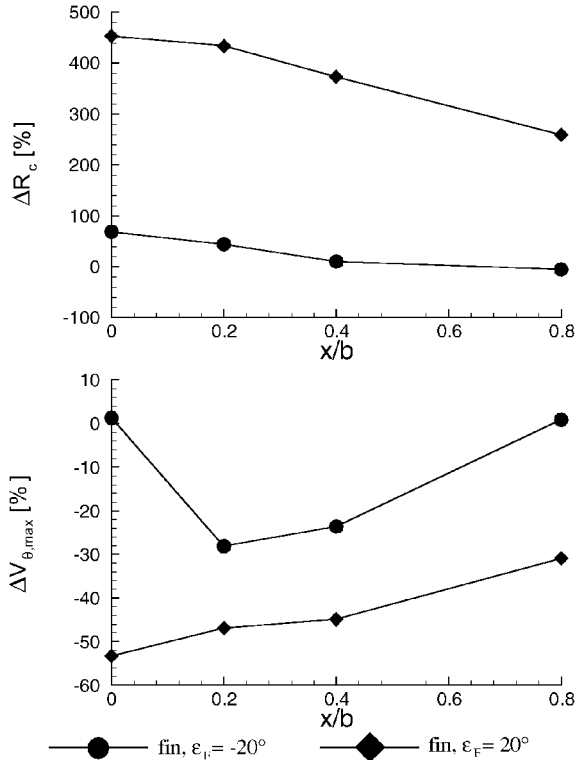

Fig. 21 Relative difference in core radius R_c and maximum tangential velocity $V_{\theta,\max}$ of outboard flap vortex caused by the wing fin.

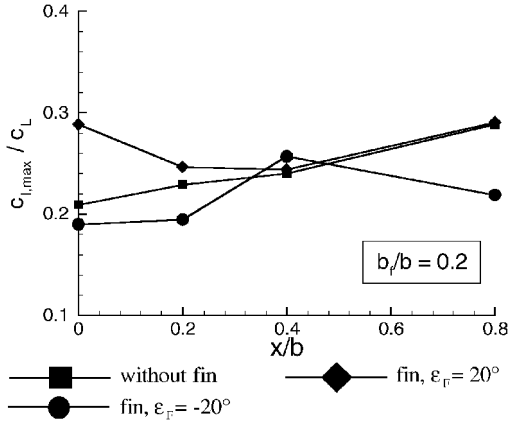

Fig. 22 Maximum induced rolling moment related to the wing lift $c_{l,\max}/c_L$ vs distance to the trailing edge x/b.

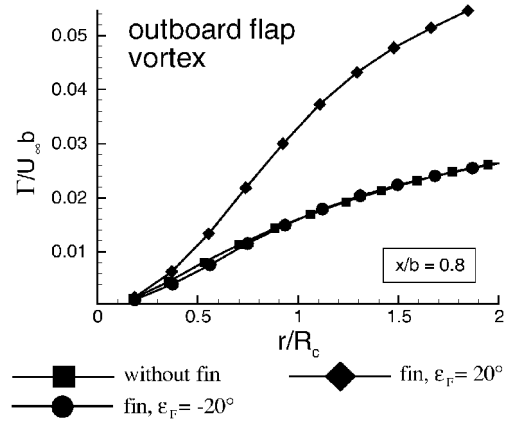

Fig. 23 Distribution of circulation $\Gamma/U_\infty\, b$ within the core of the outboard flap vortex at $x/b = 0.8$.

tangential velocity of around 40% is achieved for the configurations with fin at an angle of incidence of $\varepsilon_F = 20$ deg.

In Fig. 22 the maximum induced rolling moment related to the wing lift $c_{l,\max}/c_L$ of the investigated configurations is presented in terms of the distance to the trailing edge x/b. Only the configuration with the fin at the negative angle of incidence shows a decrease of 24% in maximum induced rolling moment $c_{l,\max}/c_L$ in the last measured plane at $x/b = 0.8$ compared to the reference configuration without fin. The configuration with fin at a positive angle of incidence does not show a change in the maximum induced rolling moment at $x/b = 0.8$ compared to the configuration without fin.

An explanation for the inefficiency of the alleviation of the maximum induced rolling moment of this configuration can be seen in Fig. 23. Because of the influence of the wing fin at $\varepsilon_F = 20$ deg, circulation is accumulated within the vortex core of the outboard flap vortex because of the rolling up of the additional positive vorticity generated by the wing fin and parts of the vorticity in the boundary

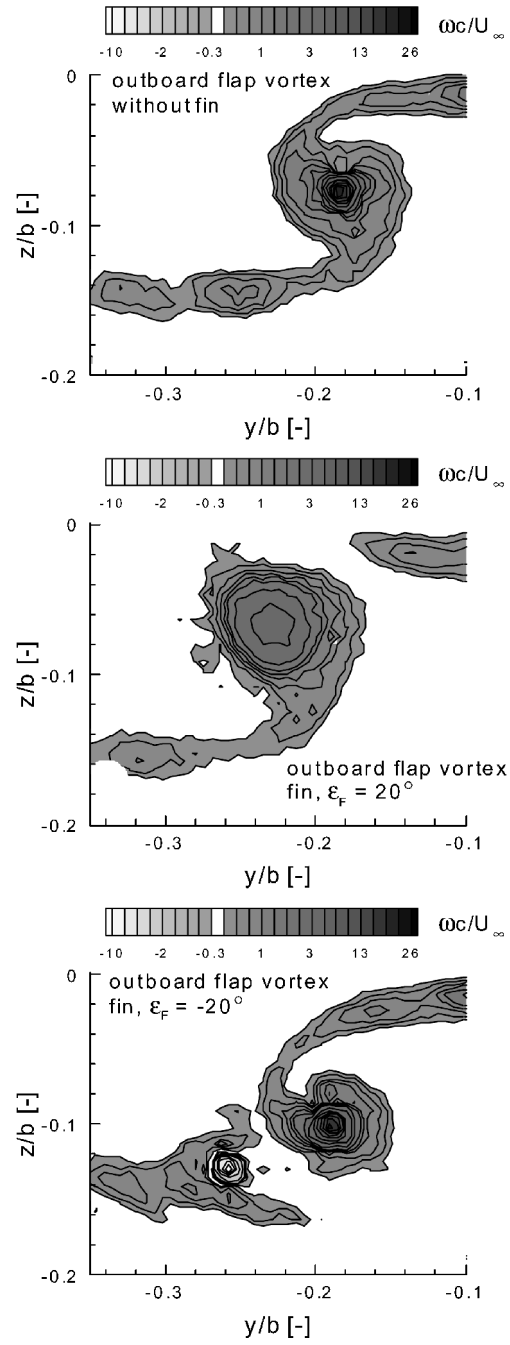

Fig. 24 Distribution of vorticity $\omega c/U_\infty$ at the outboard flap vortex at $x/b = 0.8$.

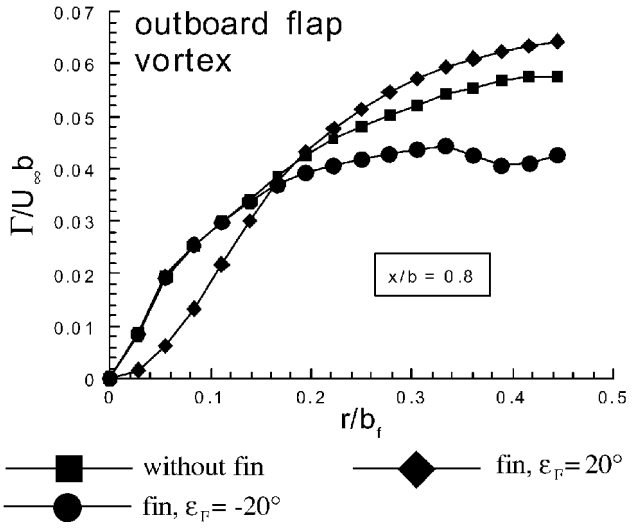

Fig. 25 Distribution of circulation $\Gamma/U_\infty\, b$ of the outboard flap vortex as a function of the dimensionless radius r/b_f at $x/b = 0.8$.

layer of the wing. The rolling up of additional vorticity compensates the alleviating effect of the widening of the flap vortex. The other fin configuration ($\varepsilon_F = -20$ deg) shows no or just a slight accumulation of circulation within the vortex core.

The influence of the angle of incidence of the fin is presented in Fig. 24, which shows the vorticity distribution in the region of the outboard flap vortex at $x/b = 0.8$. At a positive angle of incidence ε_F, the flow at the wing fin is separated because of the high local angle of attack caused by the inward directed flow on the upper side of the wing. This leads to a highly turbulent wake behind the fin, which interacts with the flap vortex diffusing the vortex core.

At a negative angle of incidence ε_F, the flow at the wing fin leads to a strong clockwise rotating fin tip vortex. Therefore the level of turbulence in the wake of the fin is much lower compared to a positive angle of incidence. The fin tip vortex wraps around parts of the vorticity of the wing boundary layer so that the circulation in the boundary layer is rolled up into both the flap vortex and the fin tip vortex. The smaller amount of circulation in the flap vortex compared to the configuration without fin causes the reduction in maximum induced rolling moment.

Figure 25 shows the circulation distributions of the flap vortex of the three cases summarizing the results mentioned before. Although the fin with positive angle of incidence ε_F diffuses the circulation within the inner part of the vortex, it fails to distribute the circulation in the outer part (from $r/b_f = 0.18$). In contrast, the fin with negative angle of incidence lowers the amount of circulation in the outer part (from $r/b_f = 0.16$) of the flap vortex, which leads to an appreciable decrease of the maximum induced rolling moment.

Conclusion

An experimental investigation of the influence of different flap settings on the wake structure and the alleviating effect of wing fins on the rolling moment induced on a following aircraft was conducted for a swept and tapered wing with slats and flaps. Vortex parameters such as core radius and maximum tangential velocity as well as vorticity and circulation distributions were investigated and presented.

The structure of the vortices shed at the wing tip and the flap edge is highly dependent on the flap angle and the angle of attack. For retracted flaps the circulation in the wake is rolled up into one tip vortex, whereas deploying the flaps leads to a division of circulation into the wing tip and flap vortex. This leads, especially for moderate flap angles, to a reduction of the maximum induced rolling moment related to the lift within the investigated wake field where no vortex merger of the tip and flap vortex occured.

The wake of the wing fin, and mounted at the outboard edge of the flap, consists of a fin tip vortex, whose sense of rotation depends on the angle of incidence, and of a highly turbulent wake. The turbulent wake interacts with the flap vortex leading to a widening of the flap vortex and therefore to a decrease of the maximum tangential velocity. A corotating fin tip vortex merges with the flap vortex leading to a large region of vorticity and turbulence. A counterrotating fin tip vortex does not merge with the flap vortex and influences the flap vortex by disturbing its roll-up process leading to a reduction of the maximum induced rolling moment at approximately one span behind the wing.

References

[1]Chow, J. S., Zilliac, G. G., and Bradshaw, P., "Near-Field Formation of a Turbulent Wing Tip Vortex," AIAA Paper 93-0551, Jan. 1993.

[2]Dacles-Mariani, J., Zilliac, G. G., Chow, J. S., and Bradshaw, P., "Numerical/Experimental Study of a Wingtip Vortex in the Near Field," *AIAA Journal*, Vol. 33, No. 9, 1995, pp. 1561–1568.

[3]Devenport, W. J., "The Structure and Development of a Wing-Tip Vortex," *Journal of Fluid Mechanics*, Vol. 312, 1996, pp 67–106.

[4]Betz, A., "Verhalten von Wirbelsystemen," *Zeitschrift für Angewandte Mathematik und Mechanik*, Bd. XII, No. 3, 1932, pp. 164–174.

[5]Donaldson, C. DuP., Snedeker, R. S., and Sullivan, R. D., "Calculation of Aircraft Wake Velocity Profiles and Comparison with Experimental Measurements," *Journal of Aircraft*, Vol. 11, No. 9, 1974, pp. 547–555.

[6]Eaton, J. A., and O' Flaherty, M. P., "Flowfield Prediction of Three-Dimensional Wing Trailing Vortices Using Advanced Turbulence Models," *AGARD 78th Fluid Dynamics, Conference Proceeding 584, Panel Symposium on the Characterization and Modification of Wakes from Lifting Vehicles in Fluids*, Trondheim, Norway, AGARD CP-584, Paper 7, May 1996, pp. 7-1–7-7.

[7]Krasny, R., "Computation of Vortex Sheet Roll-Up in the Trefftz Plane," *Journal of Fluid Mechanics*, Vol. 184, 1987, pp. 123–155.

[8]Rossow, V. J., "Extended-Betz Methods for Roll-Up of Vortex Sheets," *Journal of Aircraft*, Vol. 34, No. 5, 1997, pp. 592–599.

[9]de Bruin, A. C., Hegen, S. H., Rohne, P. B., and Spalart, P. R., "Flowfield Survey in Trailing Vortex System Behind a Civil Aircraft Model at High Lift," *AGARD 78th Fluid Dynamics, Conference Proceeding 584, Panel Symposium on the Characterization and Modification of Wakes from Lifting Vehicles in Fluids*, Trondheim, Norway, AGARD CP-584, Paper 25, May 1996, pp. 25-1–25-12.

[10]Chen, A. L., Jacob, J. D., and Savas, Ö., "Dynamics of Corotating Vortex Pairs in the Wake of Flapped Airfoils," *Journal of Fluid Mechanics*, Vol. 382, 1999, pp. 155–193.

[11]Corsiglia, V. R., and Dunham, R. E., "Aircraft Wake Vortex Minimization by Use of Flaps," edited by A. Gessow, NASA SP-409, Washington, D.C., Feb. 1976, pp. 305–338.

[12]Holbrook, G. T., Dunham, D. M., and Greene, G. C., "Vortex Wake Alleviation Studies with a Variable Twist Wing," NASA TP-2442, Nov. 1985.

[13]Hueneke, K., "Structure of a Transport Aircraft-Type Near Field Wake," *AGARD 78th Fluid Dynamics, Conference Proceeding 584, Panel Symposium on the Characterization and Modification of Wakes from Lifting Vehicles in Fluids*, Trondheim, Norway, AGARD CP-584, Paper 5, May 1996, pp. 5-1–5-9.

[14]Schell, I., Özger, E., and Jacob, D., "Influence of Different Flap Settings on the Wake-Vortex Structure of a Rectangular Wing with Flaps and Means of Alleviation with Wing Fins," *Aerospace Science and Technology*, Vol. 4, No. 2, 2000, pp. 79–90.

[15]Rossow, V. J., "Experimental Investigation of Wing Fin Configurations for Alleviation of Vortex Wakes of Aircraft," NASA TM 78250, Nov. 1978.

[16]Croom, D. R., "The Development and Use of Spoilers as Vortex Attenuators," edited by A. Gessow, *NASA Symposium on Wake Vortex Minimization*, NASA SP-409, Washington, D.C., Feb. 1976, pp. 339–368.

[17]Dunham, R. E., "Unsuccessful Concepts for Aircraft Wake Vortex Minimization," edited by A. Gessow, *NASA Symposium on Wake Vortex Minimization*, NASA SP-409, Washington, D.C., Feb. 1976, pp. 221–249.

[18]Rossow, V. J., "Inviscid Modelling of Aircraft Trailing Vortices," edited by A. Gessow, *NASA Symposium on Wake Vortex Minimization*, NASA SP-409, Washington, D.C., Feb. 1976, pp. 9–59.

[19]Rossow, V. J., Fong, R. K., Wright, N. S., and Bisbee, L. S., "Vortex Wakes of Two Transports in 80 by 120 Foot Wind Tunnel," *Journal of Aircraft*, Vol. 33, No. 2, 1996, pp. 399–406.